

Hippocampus's volume calculation on coronal slice's for strengthening the diagnosis of Alzheimer's

Retno Supriyanti, Yogi Ramadhani, Eko Wahyudi

Electrical Engineering Department, Faculty of Engineering, Jenderal Soedirman University, Purbalingga, Indonesia

Article Info

Article history:

Received May 25, 2021

Revised Nov 04, 2022

Accepted Nov 14, 2022

Keywords:

Alzheimer's diagnosing

Coronal slice

Hippocampus

MRI

Severity

ABSTRACT

Alzheimer's is one of the most common types of dementia in the world. Although not a contagious disease, this disease has many impacts, especially in socio-economic life. In diagnosing Alzheimer's and using interview techniques, physical examination methods are also used, namely using an magnetic resonance imaging (MRI) machine to get a clear image of the patient's brain condition, with a focus on the hippocampus and ventricular area. In this paper, we discuss the calculation of the volume of the hippocampus, especially the coronal slice, to provide information to doctors in making decisions on diagnosing the severity of Alzheimer's. Using the basis of volume calculations, we made a 3D visualization reconstruction of the coronal hippocampus slice area in order to make it easier for doctors to analyze the condition of the hippocampus area, which in the end will be used as a recommendation in the classification of the severity of Alzheimer's. Our experimental results show, the lower the severity, the bigger the volume, the more slices, and the longer the counting time.

This is an open access article under the [CC BY-SA](https://creativecommons.org/licenses/by-sa/4.0/) license.



Corresponding Author:

Retno Supriyanti

Electrical Engineering Department, Faculty of Engineering, Jenderal Soedirman University

Kampus Blater, Jl. Mayjend Sungkono KM 5, Blater, Purbalingga, Indonesia

Email: retno_supriyanti@unsoed.ac.id

1. INTRODUCTION

Alzheimer's disease has a record of an increase in sufferers every year; this disease will undoubtedly attack most people who have the elderly. However, this fact is inversely proportional to the availability of services provided in several health agencies. It is considered that this disease does not provide high profits, such as cancer, heart disease, kidney disease, and stroke, which are generally suffered by most people in developing countries like Indonesia. Many people with Alzheimer's are ignored. This disease will cause the sufferer to experience memory impairment, impaired judgment, decision-making, overall physical orientation, and problems with speech. This disease is divided into two subtypes based on age, namely early-onset Alzheimer's disease (EOAD) and late-onset Alzheimer's disease (LOAD). EOAD accounts for about 1% to 6% of total cases and ranges from 30 years to 60 or 65. However, LOAD is the most common form of Alzheimer's affecting humans aged 60 and 65 years. Both EOAD and LOAD are most likely to occur in people with a family history of Alzheimer's disease. As many as 60% of EOAD cases are from families with a history of Alzheimer's disease [1]. Several stages are carried out in the medical field to diagnose Alzheimer's, namely history, clinical examination, and magnetic resonance imaging (MRI) radiological support. Diagnosis based on the patient's behavior.

In radiology, MRI examination of the observed part is the hippocampus. Alzheimer's disease will experience abnormal conditions in the hippocampus. Neurodegeneration occurs in the brain, and oxidative stress is associated with an increase in amyloid beta ($A\beta$) deposits. $A\beta$ causes H_2O_2 accumulation in

hippocampal neuron cultures and neuroblastoma cultures. There is a shrinkage in the hippocampus according to the increase in the critical dementia ratio (CDR) value in people with Alzheimer's [2]. In radiological examinations, the most common observation of MRI images by radiologists is by photo printing. For simple cases, at least two photo printing sheets must be done on each axial, coronal, and sagittal cut. In complex cases, there may be more than five photo prints on each piece for observation. In low-resolution MRI machines such as those available in health services in developing countries such as Indonesia, this MRI machine has a weakness. The frequency of use is limited because machine precision needs to be maintained to decrease performance. The processing process to get the desired organ image takes a long time. For example, in the most straightforward cases, such as slight scratching of the bone, it takes up to half an hour, and in complex cases, it takes more than an hour. Every time the contrast improvement in the image is made, an additional cost must be added. This long-term research aims to develop a simple system that can be used to help doctors diagnose Alzheimer's patients based on severity. We have done some preliminary research before [3]–[6] but the research we did still covers the area that has not yet reached the volume calculation.

There is much research on Alzheimer's and its relationship to image processing. Among them are the following. Keserwani *et al.* [7] classified Alzheimer's based on the texture analysis of the hippocampus area. The hippocampus area was extracted using Gabor segmentation. Texture features are represented on a slice-by-slice basis with mean and the standard deviation of the magnitude of Gabor's response. Ozsahin *et al.* [8] uses backpropagation neural networks for automatic classification of 4 patient groups, including Alzheimer's disease, late mild cognitive impairment, early mild cognitive impairment, and significant memory concern, versus standard control on 18F-florbetapir positron emission tomography (PET) images from the Alzheimer's disease neuroimaging initiative (ADNI) database, with 100 images for each group. Bothraa *et al.* [9] developed an automated technique to detect Alzheimer's symptoms using an experimental approach. They divided their research into two parts, first is to get a dataset of ADNI disease and perform image processing on it that will be used to train the system. Furthermore, using the deep learning algorithm to detect a disease from this neuroimaging data. Giang *et al.* [10] they proposed using a fast-multiple kernel learning framework, known as fast multi kernel learning framework-dimensional reduction (fMKL-DR), to classify Alzheimer's disease (AD) patients and cancer patients. Maqsood *et al.* [11] developed an automated dementia detection and classification system. The system classifies dementia patients and identifies the four stages of dementia development. they utilize transfer learning to classify images by refining pre-trained convolutional network, AlexNet. Pelsmacker *et al.* [12] explored the influence of message as a mediator in the processing of Alzheimer's consciousness with various arguments, strength, and valence. Islam *et al.* [13] developed a classification method for 3D organ images are rotation and invariant translation. They extract a representative two-dimensional (2D) piece along the plane best symmetry of 3D images. furthermore, they use these slices to represent 3D images and uses a 20-layer deep convolutional neural network (DCNN) to perform classification tasks. Bhagyashree *et al.* [14] researched by developing software to link traumatic brain injury to the severity of Alzheimer's. Park and Moon [15] reviewed the use of MRI as a basis for supporting image processing-based Alzheimer's diagnosis. Cuthbert *et al.* [16] classified the severity of dementia using transfer learning with visual geometry group model 16 (VGG16) using fast AI. Kleij *et al.* [17] conducted a study on the accuracy of measuring brain parenchymal volume (BPV) and intracranial volume (ICV) by performing three-dimensional segmentation. Hadi *et al.* [18] proposed region-based segmentation of brain tumors using an active contour model. Wu *et al.* [19] proposed a three-dimensional network model for brain tumor segmentation by adopting an encoder-decoder structure and replacing convolution with group convolution to improve network performance. This paper will discuss calculating the hippocampus's brain volume based on the coronal slice of MRI segmentation images based on time, the value of CDR, gender, and age.

2. RESEARCH METHOD

2.1. Input data

In this research, we used input data from the open access series of imaging studies (OASIS) database. The OASIS project aims to create a set of MRI data sets that are freely accessible and free for the scientific community [20]–[21]. Figure 1 shows a sample of a coronal slice of hippocampus image data from Alzheimer's patients based on the CDR 0 to 2. A value of 0 indicates no dementia, 1 is mild dementia, and 2 is moderate dementia.

2.2. Active contour segmentation

This paper is a continuation of our previous research [4]–[6], [9], [10], where the segmentation used is the active contour segmentation discussed in the previous paper. Active contour is a segmentation method using a closed curve model that can move broader or narrower. Active contour can move broader or narrower by minimizing image energy using an external force and is also influenced by image features such as lines or edges.

2.3. Calculation of hippocampus volume on coronal slice

Volume calculation is done by first calculating the area of each segmented coronal hippocampus slice using the active contour method. The real slices of the entire brain MRI image slices are 1-256 slices with a thickness, each assumed to be 1 pixel/slice thick. Volume calculation is done by adding up the volume of each slice, which is the product of the multiplication of the hippocampus area multiplied by its thickness. A total of ± 30 slices will be identified for their width, then the volume of each slice is calculated, after which the hippocampus volume is calculated from the number of each volume per slice. The volume calculation is done using a mathematical approach, namely by adding up each segmented hippocampus slice area, then multiplying it by the slice height, which is assumed to be 1 pixel long. Based on the previous calculation, then the volume of each slice will be known. Figure 2 shows the plot of the brain MRI hippocampus volume calculation.

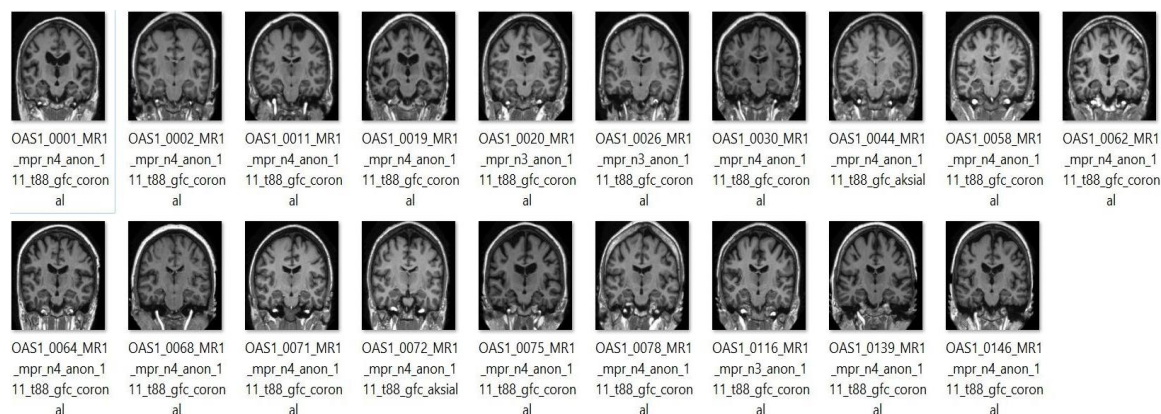


Figure 1. Coronal slice MRI image

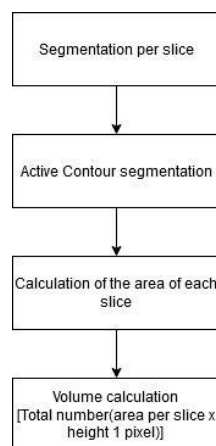


Figure 2. Flow chart of coronal hippocampus slice volume calculation

2.4. Three-dimensional visualization

Biomedical image visualization involves transformation and interaction with multi-dimensional biomedical image data sets. Researchers use several methods in creating 3D object views, which can be grouped into two techniques: surface rendering and volume rendering [22]. Surface rendering generally requires contour extraction, which is the surface of a structure to be visualized and then represented in the form of a series of polygons. A tiling algorithm is then applied to place the polygon pieces at each contour point to produce a surface appearance. The advantage of this technique is the ability to quickly generate image views for a relatively small amount of contour data. Where as the disadvantage is that it lies indiscretion when extracting contours and placing polygons on the surface, thereby reducing its accuracy [23]. Volume rendering is one of the most powerful techniques in visualization and image manipulation [24]. In this technique, there is no need for discretion from the surface so that the integrity of the volume image data is well preserved. That is why this technique can produce high-quality displays, although the implication is that the computation time is quite long.

3. RESULTS AND ANALYSIS

In this research, we used 40 MRI image data from the OASIS database. The image has identified its CDR value. The first step is to cut the image on each MRI image. The cutting was done using free software called “MRIcro.” Figure 3 shows the cut image. In coronal slices, one brain MRI consists of ± 176 2D image slices. The next step is to convert the data file, which initially has the extension “hdr” into a collection of 2D coronal brain images with the extension “.bmp.” then the results obtained are as shown in Figure 4, where in the image you can see the shape of the brain starting from the first time you can to the end of the 2D image slice.



Figure3. Display of MRIcro software

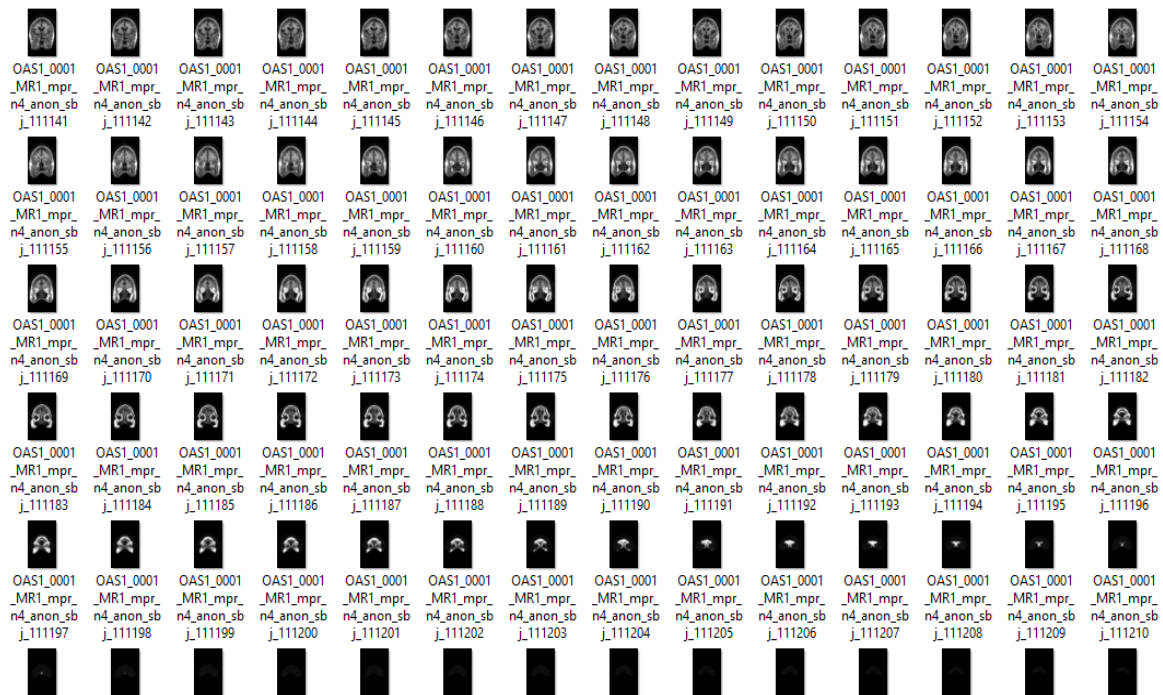


Figure 4. Coronal MRI image slice (256 slices)

As explained in section 1, this paper will discuss the calculation of the volume of the hippocampus. This discussion refers to our previous research [25]. This part of the hippocampus determines the severity of Alzheimer's. Alzheimer's disease has a small part of the hippocampus, and the size decreases over time. This part of the hippocampus was studied starting from the slice when it first appeared to the end of the hippocampus slice. In the initial process, we clustered 40 MRI brain image data, which contained a hippocampus slice. In the clustering stage, it is done manually, with the eye's help directly on the parts that have the hippocampus in it. We do this because the position of the hippocampus on each slice has different coordinates. Also, the hippocampus has a pixel intensity value that is almost the same as the other parts of the brain. Figure 5 shows an example of a successfully observed section of the hippocampus. In Figure 5(a) shows the temporal horn type of hippocampus, while in Figure 5(b) shows the middle hippocampus and in Figure 5(c) shows the hippocampus tail.

In this experiment, we clustered 40 data on MRI brain images in which there was a slice of the hippocampus. We did the clustering process manually by selecting the hippocampus directly. We use the manual method because the position of the hippocampus on each slice has different coordinates. It is also because the pixel intensity in all areas of the brain has almost the same value. Table 1 shows the results of the clusterization in this experiment.

Referring to Table 1, we see that each brain MRI has a different number of slices. On MRI images with a CDR value of 0, the number of hippocampal slices on average is more than CDR 1 and CDR 2. Likewise, CDR 1 has more average hippocampal slices compared to CDR 2. The relationship between the number of hippocampus slices on the MRI image of Alzheimer's with the CDR value is like the (1).

$$CDR\ 0 > CDR\ 1 > CDR\ 2 \quad (1)$$

In this experiment, we pre-processed all input data to get a clearer image in distinguishing between the hippocampus area and other areas. Here we use the contrast stretching method. In previous studies, the value of contrast stretching can be changed in brightness to obtain an optimal coronal hippocampus image. However, in this study, we used a controlled variable for the contrast stretching function. We do this so that there is no significant difference in pixel intensity values between one image and the next image in the initial masking process. Figure 6(a) and Figure 6(b) shows the difference in results between the original image and the image after contrast stretching.

Referring to Figure 6(a) and Figure 6(b), we can see that the image after the contrast stretching process has an even distribution of light compared to the original image. The coronal slice of the hippocampus is visible, and we can easily carry out the segmentation process. So that with the improvement of image quality using contrast stretching, the image becomes more apparent and will facilitate segmentation in the hippocampus area.

In carrying out the initial masking process, an image enlargement is carried out on the right and left hippocampus. This enlargement is done so that the contour points do not hit any part other than the coronal side's hippocampus. Because when the contour points are far from the sides of the hippocampus, the object is not appropriately segmented and can affect the volume calculation of the hippocampus. Researchers did not use the cropping command in this study because it can change the original Alzheimer's coronal MRI image size. When the size of one slice image is different from the size of another slice image, the 3D visualization formation process cannot be processed because 3D image formation requires a 3D matrix of the same size. Therefore, the zoom on and zoom off functions are used in the research.

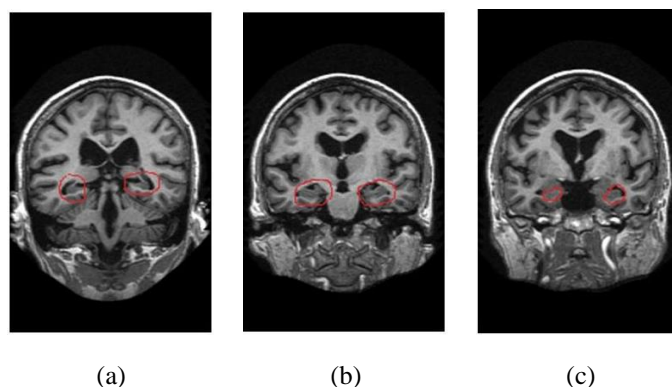


Figure 5. Hippocampus type: (a) hippocampus temporal horn, (b) hippocampus middle, and (c) hippocampus tail

The active contour process is the following process of initial masking. The segmentation with the active contour in this research is based on “edge,” which results in the contours evolving inward so that the contours are conical to form the desired object. The working principle of this active contour segmentation is that if the external energy from the contour detects a change in intensity (called edge detection), the gradient will reduce its speed to close to 0 so that the internal energy moves along the contour and forms the area of the actual object. The result of this active contour segmentation is a binary image, where the hippocampus is 1 (white) and other than that it is 0 (black) with the same size as the original MRI image, which is 208×176 pixels. The results of the initial masking will be automatically segmented using the active contour method. Figure 7 describes the results of the hippocampus segmentation in this research.

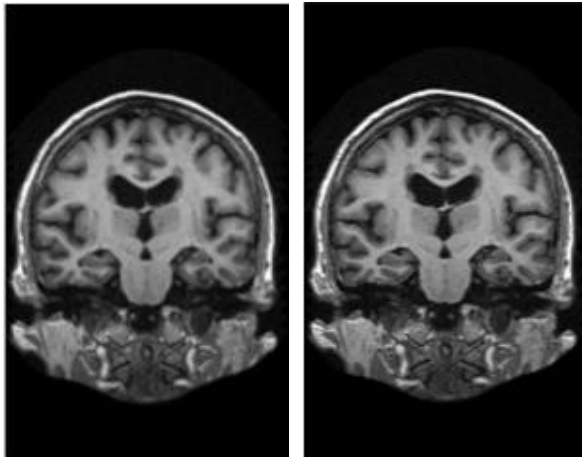
Table 1. Identification results

No	ID	Male/female	Age	CDR	Slice full	Slice hippo
1	OAS1_0058_MR1	F	46	0	256	33
2	OAS1_0044_MR1	F	47	0	256	30
3	OAS1_0020_MR1	F	48	0	256	29
4	OAS1_0011_MR1	F	52	0	256	31
5	OAS1_0002_MR1	F	55	0	256	32
6	OAS1_0026_MR1	F	58	0	256	33
7	OAS1_0030_MR1	F	65	0	256	31
8	OAS1_0001_MR1	F	74	0	256	32
9	OAS1_0033_MR1	F	80	0	256	28
10	OAS1_0019_MR1	F	89	0	256	30
11	OAS1_0069_MR1	M	33	0	256	25
12	OAS1_0018_MR1	M	39	0	256	25
13	OAS1_0074_MR1	M	43	0	256	31
14	OAS1_0034_MR1	M	51	0	256	24
15	OAS1_0114_MR1	M	62	0	256	34
16	OAS1_0135_MR1	M	64	0	256	26
17	OAS1_0130_MR1	M	68	0	256	28
18	OAS1_0010_MR1	M	74	0	256	32
19	OAS1_0110_MR1	M	84	0	256	31
20	OAS1_0065_MR1	M	90	0	256	30
21	OAS1_0184_MR1	F	65	1	256	32
22	OAS1_0382_MR1	F	67	1	256	27
23	OAS1_0067_MR1	F	71	1	256	28
24	OAS1_0056_MR1	F	72	1	256	29
25	OAS1_0269_MR1	F	72	1	256	31
26	OAS1_0316_MR1	F	72	1	256	26
27	OAS1_0052_MR1	F	78	1	256	26
28	OAS1_0053_MR1	F	83	1	256	31
29	OAS1_0035_MR1	F	84	1	256	23
30	OAS1_0430_MR1	M	71	1	256	29
31	OAS1_0424_MR1	M	75	1	256	23
32	OAS1_0452_MR1	M	75	1	256	29
33	OAS1_0405_MR1	M	77	1	256	30
34	OAS1_0268_MR1	M	78	1	256	29
35	OAS1_0399_MR1	M	78	1	256	29
36	OAS1_0134_MR1	M	80	1	256	23
37	OAS1_0223_MR1	M	84	1	256	29
38	OAS1_0031_MR1	M	88	1	256	27
39	OAS1_0308_MR1	F	78	2	256	22
40	OAS1_0351_MR1	M	86	2	256	23

Calculation of the volume of the hippocampus can be done when all coronal slice hippocampus images have been segmented thoroughly, from the first to the last slice, and entered in the same folder-then given the sequential names starting from the beginning of the emergence of the hippocampus (horn) to the end of the hippocampus (tail). This sequential naming is used to make it easier to access files in a folder so that users do not need to access images one by one, simply by selecting a folder in which there is a collection of MRI image slices. The method used to find the volume of the hippocampus is to enter a collection of images in the folder into a 3D matrix. The image used is a binary image, so the value of the hippocampus in each slice is expressed as 1 (white) and outside the hippocampus is 0 (black). So it can be concluded that the volume of the hippocampus is the addition of the 3D matrix into one 1x1 matrix. The 3D visualization process is carried out by placing each segmented 2D hippocampus slice into a 3D matrix. In this research, the zero function is used to place a 2D image into a 3D matrix. When the 2D coronal Alzheimer’s image is placed on a 3D matrix, it will look like the illustration visualization in Figure 8. This image is a display of a 2D brain slice containing the hippocampus image. Then the images are stacked into a 3D matrix.

In this research, only the hippocampus is shown in 3D, and other parts are ignored. Because the parts of the hippocampus in each coronal MRI image have been segmented in the previous processes, only part of the coronal hippocampus is automatically displayed on the screen. In the segmented image, the visualization of the 3D matrix in each stack will resemble the shape of the hippocampus itself, as shown in Figure 9.

Referring to Figure 9, then we reconstruct the 3D visualization of the previously formed 3D matrix. In this research, the results of 3D reconstruction from a collection of 2D MRI images of the hippocampus are smoothed using the smooth function; this visual refinement is functional. The image is better than the previous results, as shown in Figure 10. Figure 10 shows the results of 3-dimensional visualization, where in Figure 10(a) shows the results before smoothing implementation, while in Figure 10(b) is the result of visualization after the smoothing process.



(a)

(b)

Figure 6. Before and after contrast stretching:
(a) original image and (b) after contrast stretching

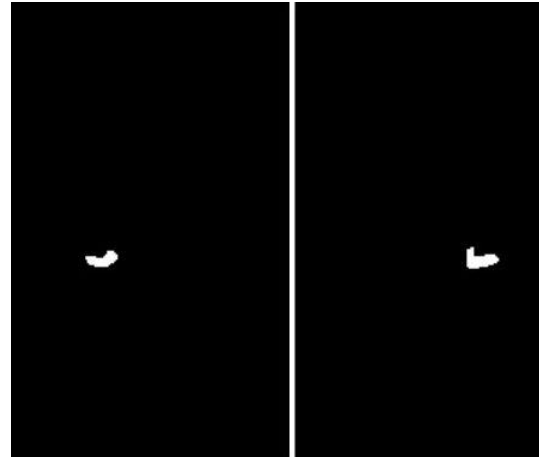


Figure 7. Segmentation result

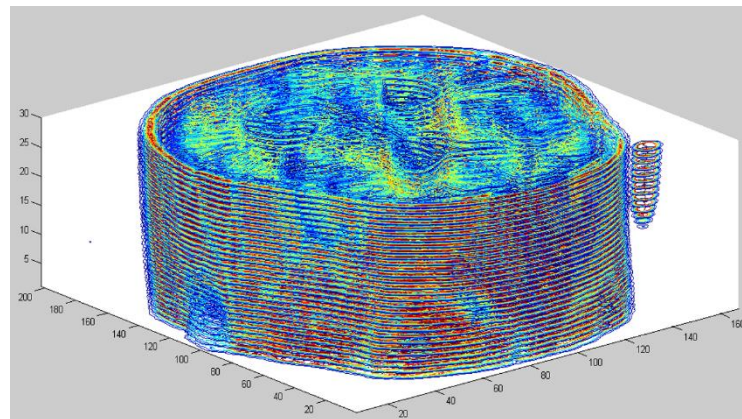


Figure 8. Alzheimer's brain coronal slice stacks

All results of the 3D visualization reconstruction of the coronal slice hippocampus image are shown in Table 2. Referring to Table 2, the relationship between volume and CDR shows that the average value for CDR 0 on the left hippocampus volume is 1973 pixels, the right hippocampus volume is 2055 pixels, and the total hippocampus volume is 4028 pixels. The average value for CDR 1 on the left hippocampus volume is 1252 pixels, the right hippocampus volume is 1253 pixels, and the total hippocampus volume is 2505 pixels. Meanwhile, the average value for CDR 2 on the left hippocampus volume is 731.5 pixels, the right hippocampus volume is 671 pixels, and the total hippocampus volume is 1402 pixels. It can be concluded that the volume of the left and right hippocampus of each hippocampus is not much different.

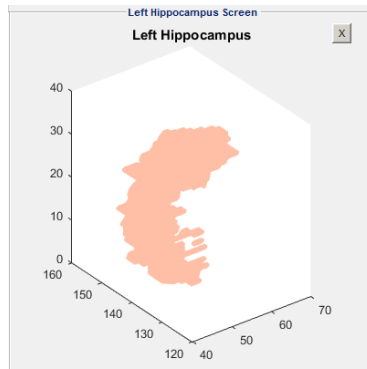


Figure 9. Hippocampus coronal slice stacks

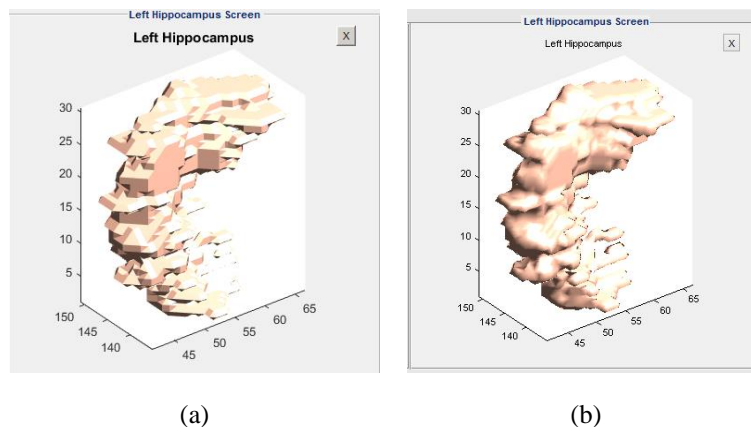


Figure 10. Hippocampus 3D visualization view (a) 3D visualisation before smoothing and (b) 3D visualisation after smoothing

Table 2. CDR VS volume of hippocampus

CDR	Left volume	Right volume	Total volume
0	1973	2055	4028
1	1252	1253	2505
2	731.5	671	1402

The relationship between CDR and the number of slices resulting from 3D visualization shows that the slices that are primarily found in CDR 0 are 30 slices, then CDR 1 is 28 slices, and CDR 2 is 23 slices. This shows that the more slices of the hippocampus's coronal MRI image, the volume will also be more significant, as shown in Table 3. In Table 3, we can see that the larger the CDR value, the smaller the number of coronal cross-sectional slices produced.

Meanwhile, the relationship between CDR and user operating time-based on 3D visualization shows that at CDR 0, the time used by the user is 74.1 minutes. CDR 1 is 66.7 minutes, and CDR 2 is 53.5 minutes. This condition shows that the lower the CDR value of an image, the longer it will calculate the volume. This condition happens because the lower the CDR value, the greater the volume and the number of slices, as shown in Table 4.

The relationship between volume and volume of the hippocampus CDR for women and men in our 3D visualization shows that the average value for the CDR 0 on the female hippocampus volume amounted to 3937 pixels, and the male hippocampus volume amounted to 4120 pixels. The average value for CDR 1 on the volume of the female hippocampus is 2421 pixels, and the volume of the male hippocampus is 2590 pixels. Furthermore, the average value for CDR 2 in the volume of the female hippocampus is 1558 pixels, and the volume of the male hippocampus is 1247 pixels as shown in Table 5.

The relationship between volume and CDR from our 3D visualization results for each age shows that at CDR 0, the older the Alzheimer's sufferer, the smaller the volume value. Meanwhile, for CDR 1 Alzheimer's sufferers starting from the age of 60 years and over. Meanwhile, CDR 2 for Alzheimer's patients starts at the age of 70 years as shown in Table 6.

Table 3. CDR VS the number of slices

CDR	The number of slices
0	30
1	28
2	23

Table 4. CDR vs time processing

CDR	Time processing
0	74.1
1	66.7
2	53.5

Table 5. Male vs female

CDR	Male himppocampus	Female hippocampus
0	3937	4120
1	2421	2590
2	1558	1247

Table 6. CDR vs age

CDR	40-50	51-60	61-70	71-80	81-90
0	4355	4642	4007	3483	3132
1	-	-	3392	2500	2076
2	-	-	-	1247	1558

4. CONCLUSION

3D visualization calculations in the hippocampus coronal slice area have different volume values. The average volume value of CDR 0 is more significant than CDR 1 and CDR 2, and the average volume value of CDR 1 is more significant than CDR 2 but is smaller than CDR 0. The value of the volume of the hippocampus is the sum of the 3D matrix from the 2D image slices of each hippocampus. The results of the 3D hippocampus visualization on each image also have a different appearance. When segmenting each 2D MRI image slice, part of the hippocampus of each image has a different shape and coordinates. The lower the CDR value, the bigger the volume and the more slices, and the calculation time by the user will be longer. The difference in the volume of the left and right hippocampus did not show a significant difference. Regarding gender, the differences in the volume of the hippocampus of men and women are relatively the same. As for age, for people with Alzheimer's, as they get old, the volume will shrink. Moreover, people with Alzheimer's with CDR 1 starting from the age of 60 years and over. Meanwhile, CDR 2 starts from the age of 70 years and over.

ACKNOWLEDGEMENTS

We would like to thank Jenderal Soedirman University through scheme "Fasilitasi Guru Besar" with contract number T/543/UN23.18/PT.01.03/2021.

REFERENCES

- [1] B. McDougall, *Understanding dementia. A guide for carers and support people*, New Zealand: Bupa Care Services NZ, 2020. [Online]. Available: <https://www.bupa.co.nz/media/15caudid/understanding-dementia-booklet-bupa-nz.pdf>
- [2] G. McKhann, D. Drachman, M. Folstein, R. Katzman, D. Price, and E. M. Stadlan, "Clinical diagnosis of Alzheimer's disease: Report of the NINCDS-ADRDA Work Group under the auspices of Department of Health and Human Services Task Force on Alzheimer's Disease," *Neurology*, vol. 34, pp. 939-944, 1984, doi: 10.1212/wnl.34.7.939.
- [3] R. Supriyanti, A. K. Marchel, Y. Ramadhani, and H. B. Widodo, "Coronal slice segmentation using a watershed method for early identification of people with Alzheimer's," *TELKOMNIKA (Telecommunication Computing Electronics and Control)* vol. 19, no. 1, pp. 63-72, 2021, doi: 10.12928/telkomnika.v19i1.15142.
- [4] R. Supriyanti, A. R. Subhi, E. J. Ashari, F. Ahmad, Y. Ramadhani, and H. B. Widodo, "Simple Classification of the Alzheimer's Severity in Supporting Strengthening the Diagnosis of Patients based on ROC Diagram," *IOP Conference Series: Materials Science and Engineering* 9, vol. 982, 2020, doi: 10.1088/1757-899X/982/1/012007.
- [5] R. Supriyanti, A. R. Subhi, Y. Ramadhani, and H. B. Widodo, "A Simple Tool for Identifying The Severity of Alzheimer's Based on Hippocampal and Ventricular Size Using A ROC Curve on a Coronal Slice Image," *Asian Journal of Information Technology*, vol. 17, pp. 321-327, 2018. [Online]. Available: <http://docsdrive.com/pdfs/medwelljournals/ajit/2018/321-327.pdf>
- [6] R. Supriyanti, "Technology supporting health services for rural areas based on image processing," *International Conference On Engineering, Technology and Innovative Researches*, 2019, vol. 1367, doi: 10.1088/1742-6596/1367/1/012090.
- [7] P. Keserwani, V. S. C. Pammi, O. Prakash, A. Khare, and M. Jeon, "Classification of Alzheimer Disease using Gabor Texture Feature of Hippocampus Region," *International Journal of Image, Graphics and Signal Processing (IJIGSP)*, vol. 8, no. 6, pp. 13-20, 2016, doi: 10.5815/ijigsp.2016.06.02.
- [8] I. Ozsahin, B. Sekeroglu, and G. S. P. Mok, "The use of back propagation neural networks and 18F-Florbetapir PET for early detection of Alzheimer's disease using Alzheimer's Disease Neuroimaging Initiative database," *PLoS One*, vol. 14, no. 12, pp. 1-13, 2019, doi: 10.1371/journal.pone.0226577.
- [9] S. Bothra, J. Jackson, and S. Telang, "Proposed System For Detection F Alzheimer's of Disease," *International Journal of Advanced Research in Computer Science*, vol. 11, no. 1, pp. 8-10, 2020. [Online]. Available: <http://www.ijarcs.info/index.php/Ijarcs/article/view/6503/5249>
- [10] T. T. Giang, T. P. Nguyen, and D. H. Tran, "Stratifying patients using fast multiple kernel learning framework: Case studies of Alzheimer's disease and cancers," *BMC Medical Informatics and Decision Making*, vol. 20, no. 108, 2020, doi: 10.1186/s12911-020-01140-y.
- [11] M. Maqsood *et al.*, "Transfer learning assisted classification and detection of alzheimer's disease stages using 3D MRI scans," *Sensors*, vol. 19, no. 11, 2019, doi: 10.3390/s19112645.
- [12] P. D. Pelsmacker, M. Lewi, and V. Cauberghe, "The Role of Affect and Cognition in Processing Messages about Early Diagnosis for Alzheimer's Disease by Older People," *Healthcare*, vol. 5, no. 2, 2017, doi: 10.3390/healthcare5020027.
- [13] K. T. Islam, S. Wijewickrema, and S. O'Leary, "A rotation and translation invariant method for 3D organ image classification using deep convolutional neural networks," *PeerJ Computer Science*, 2019, doi: 10.7717/peerj-cs.181.
- [14] S. R. Bhagyashree, Prajwalasimha S. N., Pooja B. G., and S. A. Jain, "Review on Diagnosis of Alzheimer's Disease using MRI,"

- International Journal of Innovative Research in Science, Engineering and Technology*, vol. 6, no. 1, pp. 1246–1249, 2017. [Online]. Available: http://www.ijirset.com/upload/2017/january/135_Review.pdf
- [15] M. Park and W. J. Moon, “Structural MR imaging in the diagnosis of Alzheimer’s disease and other neurodegenerative dementia: Current imaging approach and future perspectives,” *Korean Journal of Radiology*, vol. 17, no. 6, pp. 827–845, 2016, doi: 10.3348/kjr.2016.17.6.827.
- [16] M. S. Cuthbert, C. Ariza, and L. Friedland, “Feature extraction and machine learning on symbolic music using the music21 toolkit,” *12th International Society for Music Information Retrieval Conference (ISMIR 2011)*, 2011. [Online]. Available: <https://archives.ismir.net/ismir2011/paper/000090.pdf>
- [17] L. A. V. D. Kleij, J. De Bresser, J. Hendrikse, J. C. W. Siero, E. T. Petersen, and J. B. De Vis, “Fast CSF MRI for brain segmentation; Cross-validation by comparison with 3D T1-based brain segmentation methods,” *PLoS One*, vol. 13, no. 4, 2018, doi: 10.1371/journal.pone.0196119.
- [18] H. P. Hadi, E. Faisal, and E. H. Rachmawanto, “Brain tumor segmentation using multi-level Otsu thresholding and Chan-Vese active contour model,” *Telkomnika (Telecommunication, Computing, Electronics and Control)*, vol. 20, no. 4, pp. 825–833, 2022, doi: 10.12928/TELKOMNIKA.v20i4.21679.
- [19] M. Wu, H. L. Ye, Y. Wu, and J. Li, “Brain Tumor Image Segmentation Based on Grouped Convolution,” *2022 6th International Conference on Machine Vision and Information Technology (CMVIT 2022)*, 2022, vol. 2278, doi: 10.1088/1742-6596/2278/1/012042.
- [20] J. C. Morris, “The Clinical Dementia Rating (CDR): current version and scoring rules,” *Neurology*, vol. 43, no. 11, 1993, doi: 10.1212/WNL.43.11.2412-a.
- [21] A. Fotenos, A. Z. Snyder, L. E. Girton, J. C. Morris, and R. L. Buckner, “Normative estimates of cross-sectional and longitudinal brain volume decline in aging and AD,” *Neurology*, vol. 64, no. 6, 2005, doi: 10.1212/01.WNL.0000154530.72969.11.
- [22] R. A. Robb, “3-Dimensional Visualization in Medicine and Biology,” in *Handbook of Medical Imaging: Processing and Analysis*. San Diego, California: Academic Press, 2000. [Online]. Available: https://web.archive.org/web/20050601063155id_/http://www.ii.metu.edu.tr:80/~med-ii/makaleler/robb-handbook-MI-2000.pdf
- [23] K. H. Hohne and M. Bomans, A. Pommert, M. Riemer, U. Tiede, and G. Wiebecke, “Rendering Tomographic Volume Data: Adequacy of Methods for Different Modalities and Organs,” *3D Imaging in Medicine*, 1990, vol. 60, pp. 197–215, doi: 10.1007/978-3-642-84211-5_12.
- [24] R. A. Drebin, L. Carpenter, and P. Hanrahan, “Volume rendering,” *ACM SIGGRAPH Computer Graphics*, vol. 22, no. 4, pp. 65–74, 1988, doi: 10.1145/378456.378484.
- [25] R. Supriyanti, A. R. Subhi, Y. Ramadhani, and H. B. Widodo, “Coronal slices segmentation of MRI images using active contour method on initial identification of alzheimer severity level based on clinical dementia rating (CDR),” *Journal of Engineering Science and Technology*, vol. 14, no. 3, pp. 1672–1686, 2019. [Online]. Available: https://jestec.taylors.edu.my/Vol%2014%20issue%203%20June%202019/14_3_39.pdf

BIOGRAPHIES OF AUTHORS



Retno Supriyanti    is a professor at Electrical Engineering Department, Jenderal Soedirman University, Indonesia. She received her PhD in March 2010 from Nara Institute of Science and Technology Japan. Also, she received her M.S degree and Bachelor degree in 2001 and 1998, respectively, from Electrical Engineering Department, Gadjah Mada University Indonesia. Her research interests include image processing, computer vision, pattern recognition, biomedical application, e-health, tele-health and telemedicine. She can be contacted at email: retno_supriyanti@unsoed.ac.id.



Yogi Ramadhani    is an academic staff at Electrical Engineering Department, Jenderal Soedirman University, Indonesia. He received his MS Gadjah Mada University Indonesia, and his Bachelor degree from Jenderal Soedirman University Indonesia. His research interest including Computer Network, Decision Support Syetem, Telemedicine and Medical imaging. He can be contacted at email: yogi.ramadhani@unsoed.ac.id.



Eko Wahyudi    received his Bachelor degree from Electrical Engineering Department, Jenderal Soedirman University Indonesia. His research interest Image Processing field. In connection with research on image processing, several prototypes of image-based devices have been developed by the person concerned. He can be contacted at email: eko.wahyudi@mhs.unsoed.ac.id.